Hindawi Publishing Corporation
Advances in Meteorology
Volume 2013, Article ID 891260, 16 pages
http://dx.doi.org/10.1155/2013/891260

Research Article

A Comparison of Southern Hemisphere Cyclone Track Climatology and Interannual Variability in Coarse-Gridded Reanalysis Datasets

Timothy Paul Eichler[1] and Jon Gottschalck[2]

[1] *Department of Earth and Atmospheric Sciences, Saint Louis University, 3642 Lindell Boulevard, O'Neil Hall 205, St. Louis, MO 63108, USA*
[2] *NOAA/ National Weather Service, National Centers for Environmental Prediction, Climate Prediction Center, 5830 University Research Court, College Park, MD 20740, USA*

Correspondence should be addressed to Timothy Paul Eichler; teichler@slu.edu

Received 20 August 2013; Accepted 5 November 2013

Academic Editor: Igor I. Mokhov

Southern Hemisphere (SH) extratropical cyclones have received less study than their Northern Hemisphere (NH) counterparts. Generating SH cyclone tracks from global reanalysis datasets is problematic due to data reliability, especially prior to 1979. It is therefore prudent to compare the climatology and variability of SH cyclone tracks from different reanalysis datasets. We generate cyclone track frequency and intensity climatologies from three reanalysis datasets: The National Center for Environmental Prediction's Reanalysis I and Reanalysis II datasets and the European Centre for Medium Range Weather Forecasts ERA-40 dataset. Our results show that ERA-40 produces more intense cyclones in the SH active cyclone region compared to NCEP reanalyses. More intense storms are also found in the SH active cyclone region in NCEP reanalyses data post-1979 reflecting the positive trend in the AAO in the past few decades. When evaluating interannual variability, our results show Rossby wave trains including the Pacific South American (PSA) and the East Indian Ocean pattern in response to anomalous heating linked to El Niño and the Indian Ocean Dipole (IOD), respectively. Response to the AAO shows a robust annular structure for cyclone track frequency, but not intensity suggesting a weak relationship between cyclone frequency and cyclone intensity.

1. Introduction

Extratropical cyclones are an important manifestation of the Southern Hemisphere (SH) general circulation and are associated with serious socioeconomic impacts. For example, the economic costs associated with coastal cyclones in South Africa are quite large as demonstrated by infrastructure costs associated with a 2007 cyclone that resulted in R100 million along the Durban coast [1].

While cyclone tracks for the SH have been less studied than the NH, several studies have been conducted. These include those that detect cyclones in the upper levels (e.g., 300 hPa, 500 hPa) using band-passed or high-pass filtered data (e.g., Trenberth [2], J. S. Frederiksen and C. S. Frederiksen [3], Kidson and Sinclair [4], C. S. Frederiksen and J. S. Frederiksen [5], Berbery and Vera [6], Rao et al. [7], Inatsu and Hoskins [8], Nakamura and Shimpo [9], Solman and Menéndez [10], Ashok et al. [11], and Carmo and de Souza [12]). Other studies use a Lagrangian method to determine cyclones from the low levels (e.g., sea level pressure (SLP)) such as Lim and Simmonds [13], Pezza et al. [14], Pezza et al. [15], Mendes et al. [16], and Yuan et al. [17]. Hoskins and Hodges [18] utilized both Eularian and Lagrangian methods in their assessment of SH cyclone tracks. A summary of the various tracking methods is given by Neu et al. [19] who found that they were consistent, especially for deeper cyclones and also that there was no clustering among any particular tracking method.

Due to data being more sparse in the SH than the NH, SH reanalysis data is more prone to error, especially in

the pre-satellite period prior to 1979 (e.g., Bosilovich [20], Bengtsson et al. [21], Andersson et al. [22], and Chen et al. [23]). However, errors also occur for other reasons other than exclusion of satellite data alone. For instance, Rood and Bosilovich [24] found discrepancies in reanalysis datasets due to incorporation of SSM/I data. Since SH reanalysis data is more prone to error than the NH, it follows that SH cyclone tracks are also likely prone to error, although modern assimilation techniques and improved models have mitigated this issue somewhat. For example, Hodges et al. [25] evaluated SH cyclone tracks in several coarse-gridded datasets and found inconsistencies in both track density and intensity. In a follow-up paper, Hodges et al. [26] evaluated SH cyclone track climatologies among several high-resolution reanalysis datasets and found a marked improvement relative to Hodges et al. [25], with the SH cyclone track agreement approaching the NH. As stated by Hodges et al. [26], improved data assimilation, particularly with respect to satellite data, in conjunction with the use of higher resolution forecast models, directly contributed to these improvements.

When evaluating SH interannual variability of cyclone tracks, the key drivers are the position and strength of the subtropical and polar jets (STJ and SPJ, resp.). For example, Nakamura and Sampe [27], Nakamura et al. [28], and Nakamura and Shimpo [9] found a reduction in low-level extratropical cyclones under the STJ and enhanced low-level extratropical cyclones under the SPJ. Three external factors that impact the STJ and SPJ are El Niño, the Indian Ocean Dipole (IOD), and the Antarctic Oscillation (AAO). El Niño-induced changes to the SH circulation are linked to anomalous equatorial convection, which shifts the position and magnitude of the STJ and SPJ [29]. As noted by Ashok et al. [11] and found by Trenberth et al. [29], El Niño-induced changes to the general circulation are linked to the STJ and SPJ. For example, in Austral summer, the cyclone track is enhanced (suppressed) during El Niño (La Niña) due to the intensification of the STJ and SPJ during El Niño [11, 30]. Cai et al. [31] found that anomalous convection from El Niño instigates a Rossby wave train in austral winter from the central equatorial Pacific poleward, which is known as the Pacific South American (PSA) pattern [32, 33]. Cai et al. [31] also found a second Rossby wave train emanating from equatorial Africa, with centers of opposite polarity west-southwest and south of Australia, respectively. DeWeaver and Nigam [34] used NCEP reanalysis data and an Atmospheric General Circulation Model (AGCM) to also demonstrate Rossby wave propagation in response to anomalous tropical heating and cooling. It is feasible that cyclone tracks respond to midlatitude tropospheric changes from Rossby wave trains, whose source regions are the Tropics. For example, Pezza et al. [15] did a composite analysis of SH cyclone tracks using the Southern Oscillation Index (SOI) as a proxy for ENSO. They found that when the SOI is positive, there was an increase in cyclones in the Tasman Sea and in southeastern Australia. Pezza et al. [15] also found fewer cyclones in an annular pattern around Antarctica and southern South America when the SOI was positive. Both of these changes may be in response to an El Niño-induced PSA pattern.

The Indian Ocean Dipole (IOD) refers to zonal differences in SST in the tropical Indian Ocean [35]. Similar to ENSO, the IOD alters the SH general circulation via anomalous convection, except that, for the IOD, the convection originates in the tropical Indian Ocean. Saji and Yamagata [36] regressed the 200-hPa wind onto the IOD to illustrate that a Rossby wave train emanating from anomalous convection associated with the IOD was responsible for the SH extratropical structures they observed. Ashok et al. [37] associated the positive phase of the IOD with reduced rainfall in western and southern Australia, which Ashok et al. [11] linked to weaker westerlies with a weaker cyclone track over southeastern Australia. When combined with a positive phase of El Niño, Ashok et al. [11] inferred that the result would be an extremely dry winter for this region.

Motivation for studying the AAO's effects on cyclone tracks is provided by Reason and Rouault [38], who found that most wet (dry) winters over western South Africa are associated with the negative (positive) phase of the AAO. Reason and Rouault [38] concluded the mechanisms by which the AAO impacts south African precipitation involve shifts in the STJ, changes in low-level moisture flux convergence, local uplift, low-level convergence, and relative vorticity which resulted in an equatorward shift and stronger midlatitude cyclone track in South Africa in negative phases of the AAO. Pezza et al. [15] composited cyclones using AAO and found that the pattern resembled the semiannual mode (SAM). Mendes et al. [16] performed a composite analysis on cyclone tracks and the AAO and found that cyclones were more (less) frequent at high (mid-) latitudes during positive AAO.

This paper is broken down into five additional sections. Section 2 describes the datasets used. Section 3 describes the methods used for this paper while Section 4 compares the cyclone track frequency and intensity climatology between the various reanalysis datasets. Section 5 examines interannual variability via composite analysis and partial correlation to assess the change in cyclone track frequency and intensity as a function of strong El Niño-La Niña, the IOD, and the AAO. Finally, Section 6 discusses the results and provides conclusions.

2. Data

For our study, we generate cyclone tracks from three main sources of reanalysis data: (1) The National Center for Environmental Prediction (NCEP) reanalysis I from 1950 to 2010 [39, 40] (2) NCEP reanalysis II data from 1979 to 2010 [41], and (3) The ECMWF ERA-40 reanalysis dataset from 1958 to 2001. [42]. Although we are utilizing older, coarse-gridded datasets, a key advantage of using them is their temporal extent, which is needed for the composite analysis portion of this work. Ashok et al. [11] noted that their data was limited to the 1979–2003 period, which is of relatively short temporal scale. We also wish to focus on cyclone track differences that are due to data assimilation, response to external climate forcing, and changes in climate rather than resolution differences, which makes the choice of the coarse-grid datasets attractive. Performing our analyses on the coarse-gridded dataset also provides a baseline for future work where we focus on

the impacts of spatial resolution on the interannual variability of cyclone tracks. Brief descriptions of the datasets used in our study are as follows.

(a) NCEP Reanalysis I Data. As described by Kalnay et al. [39] and Kistler et al. [40], NCEP reanalysis I data is based on the T62 version of NCEP's global spectral model with 28 vertical levels. The data was assimilated via a three-dimensional variational (3DVAR) scheme [43]. For generating storm tracks, we utilized 6 hourly sea-level pressure (SLP) data from 1950 through 2010, with a spatial resolution of 2.5°× 2.5° (lat/lon).

(b) NCEP Reanalysis II Data. Similar to NCEP reanalysis I data, NCEP reanalysis II data is also based on the T62 version of NCEP's global spectral model with 28 vertical levels [41]. In this sense, NCEP reanalysis II data should be considered as an upgrade over reanalysis I data, instead of as a separate reanalysis data. As described by Kanamitsu et al. [41], errors that were fixed from reanalysis I data include the following: (1) reanalysis II data fixed a Southern Hemisphere bogus data (PAOBS) issue from 1979 to 92, (2) fixed a snow cover analysis error appearing from 1974 to 94, (3) repaired humidity diffusion to remove "spectral snow" issue, (4) fixed oceanic albedo for the entire period, (5) removed discontinuities in relative humidity-cloudiness relationship table at 0° and 180° for the entire period, and (6) fixed snowmelt term for the entire period. Storm tracks were generated from NCEP's reanalysis II data from 6 hourly sea-level pressure (SLP) data for 1979 through 2010, with a spatial resolution of 2.5°× 2.5° (lat/lon).

(c) ECMWF ERA-40 Data. As described by Uppala et al. [42], ERA-40 data is based off of the T159 version of the ECMWF model, with 60 vertical layers. Similar to NCEP reanalyses I and II data, ERA-40 data was also assimilated via a 3DVAR scheme [44]. Similar to NCEP reanalyses I and II datasets, we also generated storm tracks from ERA-40 data, and we generated storm tracks from 6 hourly sea-level pressure (SLP) data with a spatial resolution of 2.5°× 2.5° (lat/lon). The time period we chose for our ERA-40 climatology was from 1958 to 2001.

3. Methods

We generate storm tracks using the method developed by Serreze [45], which identifies storms via identifying localized minima in SLP relative to surrounding grid points. For this study, we utilize a 1 hPa threshold, which is identical to that used by Eichler and Higgins [46]. To allow for "center jumps," the maximum distance a storm may move between time steps is 800 km. This method was employed by Eichler and Higgins [46] to generate a North American climatology from NCEP/NCAR reanalysis I six hourly SLP data from 1950 to 2002. In our study, we extend the climatology developed from NCEP reanalysis I data by Eichler and Higgins [46] through the year 2010 (NCEP1_5010). Note that the years included are designed to be consistent with years available for assessing interannual variability. In addition, data availability was less

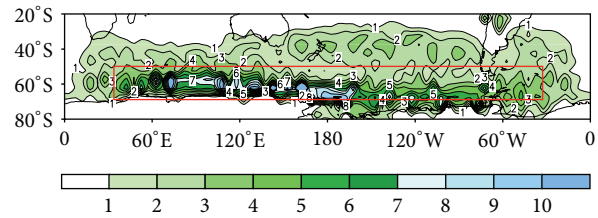

Figure 1: Area (red rectangle) chosen for analysis of differences between reanalysis datasets shown in Table 2. NCEP1_5010 used for template.

Table 1: Cyclone track climatology reanalysis datasets.

Dataset	Abbreviation used in study
Reanalysis I (1950–2010)	NCEP1_5010
Reanalysis I (1958–2001)	NCEP1_5801
Reanalysis I (1979–2010)	NCEP1_7910
Reanalysis I (1950–1978)	NCEP1_5078
Reanalysis II (1979–2010)	NCEP2_7910
ECMWF Reanalysis (1958–2001)	ERA40_5801

Note that abbreviations include the beginning and end year of the dataset (e.g., NCEP1_5010 represents reanalysis I data from 1950 to 2010).

prior to 1950 than after 1950 (e.g., see Figure 1 in Kistler et al. [40]). We also develop climatologies from ECMWF ERA-40 data from 1958 to 2001 (ERA40_5801) and NCEP reanalysis II data from 1979 to 2010 (NCEP2_7910).

Since data prior to 1979 suffers from greater uncertainty due to the lack of inclusion of satellite data, we split the reanalysis I data into two sections: the first from 1950 to 1978 (NCEP1_5078) and the second from 1979 to 2010 (NCEP1_7910). By doing this, we can compare the pre-satellite and post-satellite eras to check for discrepancies. This also allows us to assess for potential climate signals such as from trends in the AAO [47]. The reanalysis I data from 1979 to 2010 is also used to evaluate if improvements made in the reanalysis II data impacts cyclone track climatology. To make a comparison with ERA40_5801, we also develop a climatology from NCEP reanalysis I data from 1958 to 2001 (NCEP1_5801). All reanalysis datasets and their abbreviations used in this study are summarized in Table 1.

Cyclone track climatologies were generated by binning cyclone frequency and intensity into 5° latitude × 5° longitude boxes similar to Eichler and Higgins [46]. To account for latitudinal dependence, we generated a seasonal MSLP climatology for each reanalysis dataset from monthly MSLP data and detrended by performing a gridded linear regression. We then normalized the cyclone track intensity by subtracting the detrended seasonal MSLP for each grid box. In each case, we used a representative climatology to ensure consistency (e.g., ERA40_5801 climatology was subtracted from ERA40_5801 cyclone intensity, NCEP1_7910 climatology was subtracted from NCEP1_7910 cyclone intensity, etc.). Results are presented for each season defined for austral summer (JFM), austral fall (AMJ), austral winter (JAS), and austral spring (OND). Since SH cyclone tracks decrease in

Table 2: Years used in composite study for El Niño, NAO, and IOD (JFM except OND for IOD).

El Niño	1950, 1958, 1966, 1969, 1973, 1983, 1987, 1992, 1998, and 2010
La Niña	1950, 1971, 1974, 1976, 1989, 1999, 2000, and 2008
Positive IOD	1951, 1956, 1959, 1962, 1963, 1968, 1970, 1974, 1976, 1982, 1986, 1996, 1998, 2000, and 2001
Negative IOD	1950, 1957, 1964, 1965, 1966, 1969, 1971, 1972, 1975, 1978, 1980, 1983, 1985, and 2005
Positive NAO	1950, 1957, 1959, 1961, 1967, 1973, 1974, 1976, 1983, 1989, 1990, 1992, 1993, 1994, 1995, 1997, 1998, 2000, 2002, and 2008
Negative NAO	1955, 1963, 1969, 1979, 1985, 1996, and 2010

frequency equatorward of the high midlatitudes, we assess cyclone track frequency and intensity differences for the SH active cyclone track region (52.5°S–67.5°S, 32.5°E–37.5°W) for JAS as indicated in Figure 1. Unlike their NH cyclone track counterparts, SH cyclone track intensity and frequency are fairly well collocated, justifying our choice for one area to assess frequency and intensity differences. Cyclone track frequency and intensity are averaged over this region and differenced using the respective reanalysis datasets described above. Statistical significance is tabulated by utilizing a student t-test.

Although we acknowledge the potential for additional error by including some data from pre-1979, we prefer to take the approach of Hoskins and Hodges [18], who used the entire temporal period of data to assess SH cyclone tracks. The advantage is that we can generate statistics for a longer time period. Hoskins and Hodges [18] evaluated the impact of changes to the observing system on their results and determined that the lack of satellite data did not significantly alter their conclusions.

For the interannual variability portion of this work, we chose to focus on El Niño, the IOD, and the AAO. A composite analysis was performed to investigate the behavior of cyclone track intensity and frequency during extreme climate regimes. We chose to focus on SH winter (JAS) for our composite analysis, since cyclone tracks are most enhanced in SH winter (e.g., see Hoskins and Hodges [18]). Since the IOD impacts are the strongest in SH Spring, IOD composites were computed for OND.

For our ENSO composites, we used the ENSO Intensity Index (EIS) described in Kousky and Higgins [48], which is calculated by doubling the Ocean Niño Index (where the Ocean Niño Index or ONI is defined as the three-month running mean of the Niño3.4 index) to determine El Niño and La Niña periods. Moderate/strong El Niño (La Niña) events were defined by EIS greater than or equal (less than or equal) to two (negative two). For the AAO, we utilized the SH Annular Mode Index (SAMI) from Nan and Li [49], which calculates AAO by taking the normalized difference in SLP between 40°S and 70°S. This slightly differs from the traditional method of differencing 40°S and 65°S used by Gong and Wang [50]. Nan and Li [49] chose to use 70°S because of a more robust negative correlation between 40°S and 70°S as opposed to 40°S and 65°S. For IOD, we utilized data from Saji et al. [35].

Compositing the AAO and IOD was done according to standard deviation (SD). We utilized a 75 SD cutoff for positive and negative AAO and IOD events to preserve sample size and to provide an appropriate level to detect potential climate signals.

Composite analysis is shown only for NCEP1_5801 and ERA40_5801 to highlight potential differences between ERA-40 and NCEP reanalysis datasets. A reason for not showing other reanalysis datasets is that they are of insufficient temporal length. We also chose not to show NCEP1_5010, since it is contains a large amount of overlap with NCEP1_5801.

While composite analysis gives a perspective on how cyclone tracks respond to strong ENSO, IOD, and AAO events, there is a risk of external influences from other external climate forcing. We therefore employ a partial correlation analysis. As described by Ashok et al. [11], partial correlation eliminates the potential effects of variable "A_3" when correlating variables "A_1" with "A_2." It is also feasible to extend this method to four variables to eliminate the effects of "A_1" and "A_2" when correlating "A_3" with "A_4." We employ partial correlation for both three and four variables. For our study, we correlate El Niño eliminating IOD and IOD eliminating El Niño. Since IOD and El Niño represent external forcing of the climate system and the AAO represents internal variability of the climate system, we did not eliminate AAO in our IOD/El Niño partial correlation analysis. However, for the AAO correlations, we eliminated El Niño and the IOD as potential contributors to our results. Sufficient temporal size allows us to include a comparison between NCEP1_7910 and NCEP1_5078.

4. Climatology

Seasonally averaged cyclone track frequency and intensity for NCEP1_5010 are shown in Figure 2. Note that since cyclone track frequency and intensity climatologies in our other datasets are qualitatively similar to those described here, they are shown in Figures 9 and 10, respectively. NCEP1_5010 shows an increase in frequency from Austral summer to winter, with a decrease in Austral Spring poleward of the Antarctica coast, consistent with Simmonds et al. [51], Hodges et al. [25], and Hoskins and Hodges [18] (Figures 2(a)–2(d)). We also note that the area from the South Indian Ocean eastward to south of Australia has the largest number of storms in agreement with Simmonds et al. [51] and Ulbrich et al. [52]. The frequency maxima near the coast of Antarctica are attributed to the large baroclinicity in that region [25, 53]. The potential differences due to either tracking methodology and/or spatial resolution are noted by our frequency magnitudes being somewhat less than those of Hodges et al. [25] and Hoskins and Hodges [18]. A possible cause is tracking methodology, since Hoskins and Hodges [18] used ERA-40 data in their analysis. However, data resolution may also play a role. For example, Akperov and Mokhov [54] compared NH storm tracks between NCEP reanalysis I, ERA-40, and ERA-INTERIM data and found a greater number of storms with radii less than 200 km in

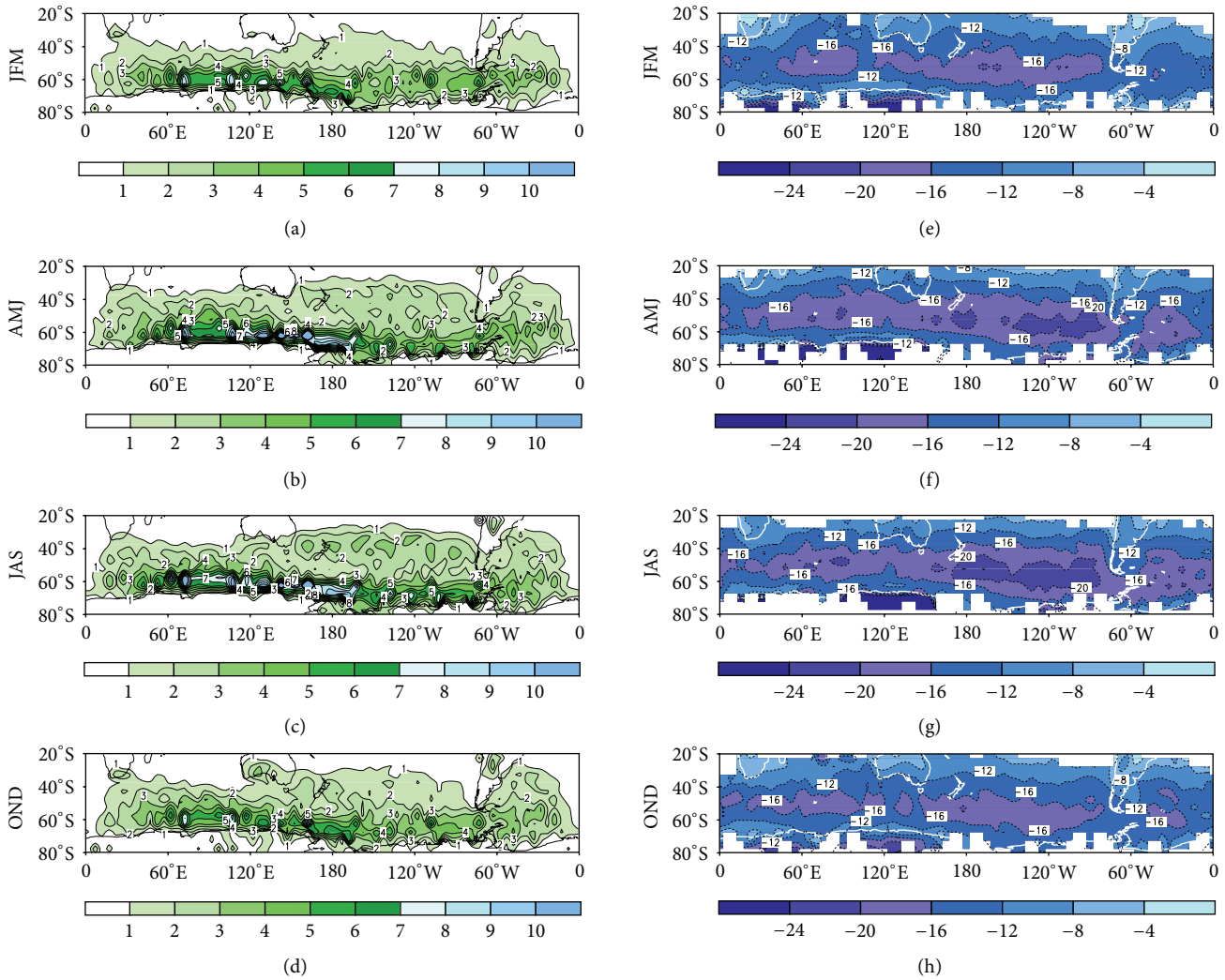

FIGURE 2: Southern Hemisphere seasonal cyclone track frequency climatology for NCEP1_5010 for (a) JFM, (b) AMJ, (c) JAS, (d) OND Units: seasonally averaged mean number of storms per 5°Lat/5° Lon grid box. Southern Hemisphere seasonal cyclone track intensity climatology per 5°Lat/5° Lon grid box for NCEP1_5010 for (e) JFM, (f) AMJ, (g) JAS, and (h) OND. Intensity calculated relative to seasonal mean sea-level pressure climatology for a unit: hPa.

the ERA-INTERIM data due to the ability of the ERA-INTERIM data to resolve cyclones of smaller spatial scale. Tilinia et al. [55] also found that cyclone frequency increased as a function of spatial resolution, with numbers increasing from 1390/yr in reanalysis II data to more than 1800/year. in the high-resolution NASA MERRA data. Interestingly, Tilinia et al. [55] also found that tracking methodology did play a role in cyclone frequency when examining rapidly deepening cyclones.

For cyclone intensity, NCEP1_5010 produces increasingly intense cyclones from austral summer to austral winter, with a trend towards less intense cyclones in austral spring (Figures 2(e)–2(h)). Interestingly, the most intense cyclones are located approximately 10 degrees equatorward of the most frequent cyclones similar to the findings of Hodges et al. [25], Simmonds et al. [51], and Hoskins and Hodges [18] (e.g., for Austral Winter, the most frequent cyclones are in a band centered at 60°S, while the most intense cyclones are in a band centered at 50°S (compare Figure 2(c) with Figure 2(g)). A possible reason is given by Hoskins and Hodges [18], who determined that the areas equatorward of maximum cyclone density were areas of genesis while areas closest to Antarctica were most often areas of lysis.

Although all reanalysis intensity and frequency climatologies look qualitatively similar (see Figures 9 and 10), it is prudent to evaluate differences in the SH active cyclone track during JAS (Table 3). While there is good agreement when comparing similar reanalysis products from the same time period (e.g., NCEP2_7910 versus NCEP1_7910), there are significantly less cyclones when comparing different time epochs (e.g., NCEP1_7910 compared to NCEP1_5078 (Table 3)). Although these differences may be due at least in part to comparing pre- to post-satellite periods, the differences are consistent with the positive trend in the AAO observed since the 1970s [47]. This idea is strengthened by the results of Mendes et al. [16] and Pezza et al. [15], who

Table 3: Differences between reanalysis datasets and their significance for SH active cyclone track region (32.5°E–42.5°W, 52.5°S–67.5°S) for (a) frequency and (b) intensity.

(a)

Reanalysis dataset	Frequency difference	t-value	2-tail 90% significant?
NCEP1_7910-NCEP2_7910	−.03	.4	N
NCEP1_7910-NCEP1_5078	−.57	5.97	Y
NCEP1_5801-ERA40_5801	.12	1.26	N

(b)

Reanalysis dataset	MSLP difference	t-value	2-tail 90% significant?
NCEP1_7910-NCEP2_7910	.25	.62	N
NCEP1_7910-NCEP1_5078	−1.97	3.06	Y
NCEP1_5801-ERA40_5801	3.9	7.46	Y

composited cyclone tracks with respect to AAO and found an increase just north of Antarctica and a decrease equatorward when differencing positive and negative AAO phases.

When evaluating intensity in the active SH cyclone region, significant differences occur. For example, ERA40_5801 produces significantly stronger cyclones than NCEP1_5801 (Table 3). Since both of these datasets are evaluated over identical time periods, it is likely that different assimilation techniques between the NCEP1_5801 and ERA40_5801 data are the cause. Note that, for the NH (not shown), there is excellent agreement between NCEP1_5801 and ERA40_5801 in both frequency and intensity. The agreement between NCEP2_7910 and NCEP1_7910 (Table 3) is not surprising, since NCEP2_7910 can be considered an improved version of NCEP1_7910 rather than a new completely independent reanalysis dataset. NCEP1_7910 produces more intense cyclones relative to NCEP1_5078 (Table 3), which is consistent with a positive AAO trend discussed previously when evaluating cyclone track frequency differences.

5. Interannual Variability

5.1. Composite Analysis. For our composite analysis, we choose to compare ERA40_5801 with NCEP1_5801 to assess differences between ERA-40 and NCEP reanalysis data. We chose not to perform composite analysis on NCEP1_7910, NCEP1_5078, and NCEP2_7910 because their limited temporal size, although we do include these datasets in the correlation analysis to follow.

Winter cyclone track frequency differences between El Niño and La Niña for JAS are shown for NCEP1_5801 and ERA40_5801 (Figures 3(a) and 3(b), resp.). Four primary bands are evident for both reanalysis datasets for El Niño. The first is a zone of increased cyclone frequency in the South Pacific from 35°S, 180°E east-southeastward into the South Atlantic at 50°S 40°W. Less frequent cyclones are seen equatorward generally from 45°S 50°E to 65°S 70°W. Southward from this area, more frequent cyclones stretch from 60°S 70°E eastward to 65°S 170°W. Finally, less frequent cyclones occur along the Antarctic coast from 70°E to 160°E.

The decrease (increase) in cyclones frequency in the high (mid-) latitude South Pacific, especially in austral winter is consistent with the PSA pattern discussed by Garreaud and Battisti [33] and Cai et al. [31]. The PSA consists of a Rossby wave train emanating south and southeastward from convection in the central equatorial Pacific. The area of high cyclone frequency south of Australia at 60°S is consistent with a second Rossby wave pattern originating in equatorial Africa [31].

While the overall ENSO response is similar in both reanalysis datasets, differences are also noted. For example, significantly fewer cyclones occur south of the southern tip of South America for El Niño relative to La Niña in ERA40_5801 but not in NCEP1_5801 (compare Figure 3(a) with Figure 3(b)). An increase in cyclones in El Niño relative to La Niña occurs from 65°S 160°E southeastward to 75°S 140°W in ERA40_5801, while this area is displaced eastward along 60°S in NCEP1_5801 (compare Figure 3(a) with Figure 3(b)). Significantly less frequent cyclones are also noted south of southeastern Australia in NCEP1_5801 but not in ERA40_5801 (compare Figure 3(a) with Figure 3(b)). Since the above differences are found between two different reanalysis datasets, data assimilation and model differences are the likely causes.

For ENSO intensity composites for NCEP1_5801 and ERA40_5801 (Figure 3(c) and Figure 3(d), resp.), a distinct couplet appears in the central South Pacific with stronger (weaker) cyclones from 30°S–45°S (55°S–65°S) for El Niño relative to La Niña. The couplet is better defined in NCEP1_5801 than in ERA40_5801 (compare Figure 3(c) with Figure 3(d)). A broken band of less intense cyclones also extends from south of South Africa to southern Australia, especially for NCEP1_5801 (compare Figure 3(c) with Figure 3(d)). The ENSO intensity composite is generally of opposite sign with respect to the ENSO frequency composite (compare Figures 3(a) and 3(b) with Figures 3(c) and 3(d)), implying that areas of more (less) frequent cyclones are also more (less) intense. This is consistent with alterations of the jetstream associated with ENSO-induced changes to the PSA pattern.

As was the case for El Niño, the IOD frequency composites show some interesting features (Figures 4(a) and 4(b)). We show results for austral spring (OND) since it is more favorable for IOD impacts relative to other seasons. Two broken bands oriented from west-northwest to east-south-east

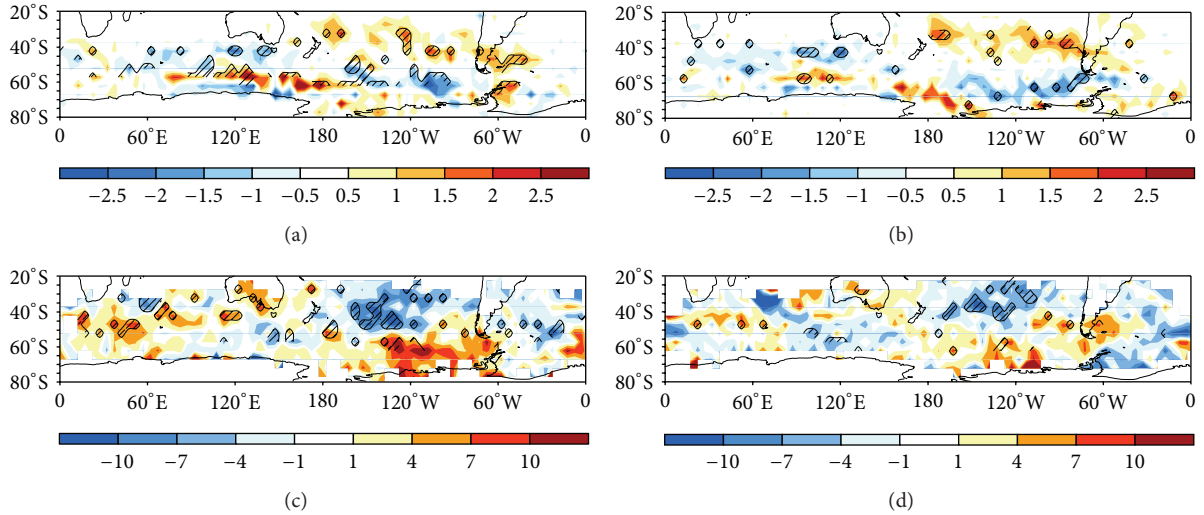

Figure 3: SH winter (JAS) El Niño-La Niña cyclone track frequency composite for (a) NCEP1_5801, (b) like "a" but for ERA40_5801. Units number of cyclones. Hatched areas are significant at 90% for 2-tailed t-test. (c) SH winter (JAS) El Niño-La Niña cyclone track intensity composite for NCEP1_5801, (d) like "c" but for ERA40_5801. Units: hPa. Hatched areas are significant at 90% for 2-tailed t-test.

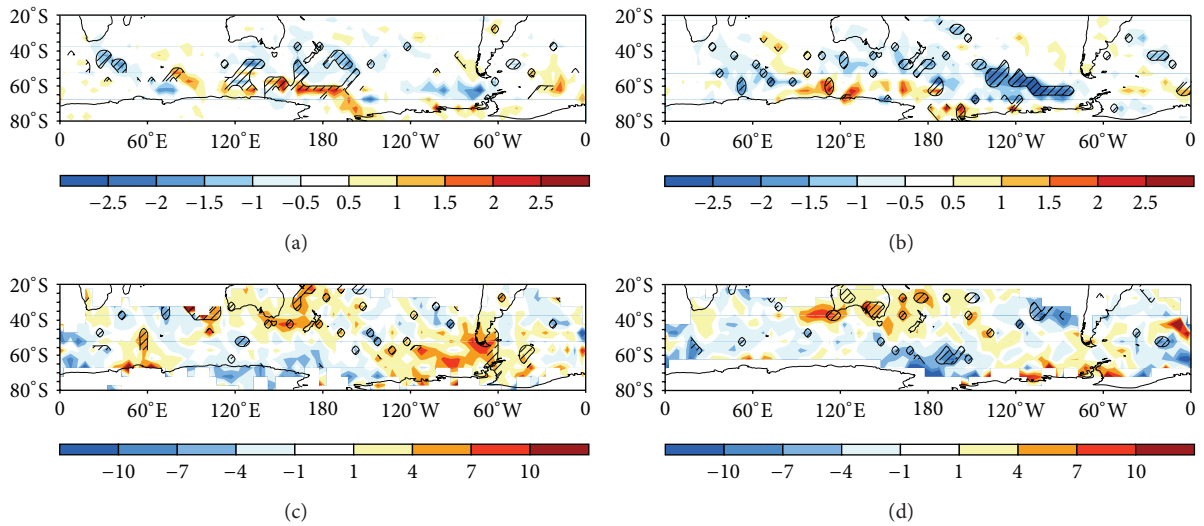

Figure 4: SH Spring (OND) IOD positive-IOD negative cyclone track frequency composite for (a) NCEP1_5801, (b) like "a" but for ERA40_5801. Units: number of cyclones. Hatched areas are significant at 90% for 2-tailed t-test. (c) SH Spring (OND) IOD positive-IOD negative cyclone track intensity composite for NCEP1_5801 (d) like "c" but for ERA40_5801. Units: hPa. Hatched areas are significant at 90% for 2-tailed t-test.

are noted in both reanalysis datasets (Figures 4(a) and 4(b)). The first band is a zone of increased cyclone frequency for positive IOD relative to negative IOD from 50°S, 90°E to 75°S, 150°W (Figures 4(a) and 4(b)). A band of decreased cyclone track frequency for positive IOD relative to negative IOD extends from 45°S, 120°E to 65°S, 70°W. The banded structure we see in austral spring is not surprising, since this is when the IOD impact is strongest [56].

The IOD frequency composite pattern is somewhat similar to the two bands between Australia and Antarctica in the ENSO composite (e.g., compare Figure 3(a) with Figure 4(a) and Figure 3(b) with Figure 4(b)), suggesting that Rossby wave propagation from the central equatorial Pacific and equatorial Africa may play a role [31]. This possibility is strengthened by the fact that IOD and ENSO are positively correlated in austral spring [31].

Consistent with the ENSO composites, regional differences occur when comparing NCEP1_5801 with ERA40_5801. For example, the band of decreased cyclones is much more prominent and significant in the South Pacific Ocean in ERA40_5801 than in NCEP1_5801 (compare Figure 4(a) with Figure 4(b)). A suggestion of a third band of decreased frequency for positive IOD relative to negative IOD is also seen in ERA40_5801 from 30°S, 50°W to 50°S, 10°W, which is only barely discernable in NCEP1_5801 (compare Figure 4(a) with Figure 4(b)).

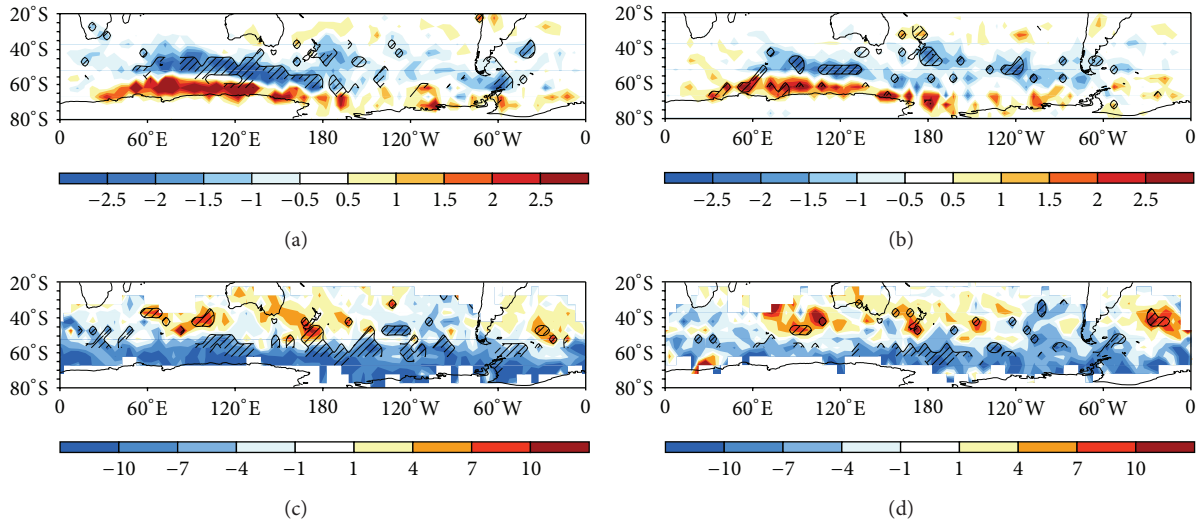

Figure 5: SH Winter (JAS) AAO positive-AAO negative cyclone track frequency composite for (a) NCEP1_5801, (b) like "a" but for ERA40_5801. Units: number of cyclones. Hatched areas are significant at 90% for 2-tailed t-test. (c) SH Winter (JAS) IOD positive-IOD negative cyclone track intensity composite for NCEP1_5801, (d) like "c" but for ERA40_5801. Units: hPa. Hatched areas are significant at 90% for 2-tailed t-test.

For the IOD cyclone track intensity, the overall structure is less defined than the IOD frequency composite. However, there is a tendency for less (more) intense cyclones south of Australia from 30°S–45°S (55°S–65°S) for positive IOD relative to negative IOD, possibly associated with changes in cyclone intensity due to Rossby wave propagation from the central equatorial Pacific and equatorial Africa.

Given that the IOD intensity composites are relatively weak, it is difficult to detect differences between NCEP1_5801 and ERA40_5801. More intense cyclones for positive IOD relative to negative IOD are seen in ERA40_5801 over the southwestern South Pacific from 55°S to 70°S and the southeastern South Pacific from 30°S to 45°S in ERA40_5801, but this is not the case for NCEP1_5801 (compare Figure 4(c) with Figure 4(d)). Less intense cyclones for positive IOD relative to negative IOD also occur between South America and Antarctica for NCEP1_5801, but not for ERA40_5801 (compare Figure 4(c) with Figure 4(d)).

The most robust results, with the largest areas of significance are for AAO composites. Our AAO frequency composites, which is calculated by subtracting the negative phase of the AAO from the positive phase of the AAO, consist of an annular structure, with increased cyclone frequency along 65°S and decreased frequency along 50°S for both datasets (Figures 5(a) and 5(b)), especially from the Indian Ocean eastward to south of Australia. Although the AAO signal is distinct for both NCEP1_5801 and ERA40_5801, the positive/negative frequency couplet for positive AAO relative to negative AAO is better defined and larger in aerial extent in NCEP1_5801 than in ERA40_5801 (compare Figure 5(a) with Figure 5(b)). The band of decreased cyclone frequency for positive AAO relative to negative AAO also extends westward to the south of South Africa in NCEP1_5801, but not in ERA40_5801 (compare Figure 5(a) with Figure 5(b)).

Interestingly, the AAO intensity composite does not line up well with the AAO frequency composite (Figures 5(c) and 5(d)). For example, while areas of more frequent and more intense cyclones line up well along 65°S, more intense cyclones extend equatorward beyond this zone to approximately 50°S, especially when examining the Indian Ocean (compare Figures 5(a) and 5(b) with Figures 5(c) and 5(d)). This implies that fewer (greater), but more (less), intense cyclones occur in the South Indian Ocean in the vicinity of 50°S during positive (negative) AAO. While this may seem surprising, Pezza et al. [15] points out that Simmonds [57] did not find a strong correlation between SLP and cyclone intensity. As noted in Section 3, the fact that areas equatorward of maximum cyclone density were areas of genesis while areas closest to Antarctica were most often areas of lysis may also play a role [18]. Although beyond the scope of this paper, it would be interesting to investigate the locations of genesis and lysis in the South Indian Ocean to further explore how they map onto the AAO.

The above results show some interesting responses that cyclone track frequency and intensity have with respect to distinct phases of ENSO, the IOD, and the AAO. We see structures that map well to Rossby wave trains triggered by anomalous convection. We also see differences due to varying assimilation processes between the NCEP and ER40 reanalysis datasets. The sensitivity of regional response to choice of reanalysis products suggests that caution should be observed when evaluating interannual variability on a regional domain. Since we cannot eliminate contamination from other climate forcing as contributing to our results (e.g., ENSO influencing IOD), we perform a partial correlation analysis in the next section.

5.2. Partial Correlation Analysis. In this section, we employ partial correlation analysis similar to Ashok et al. [11],

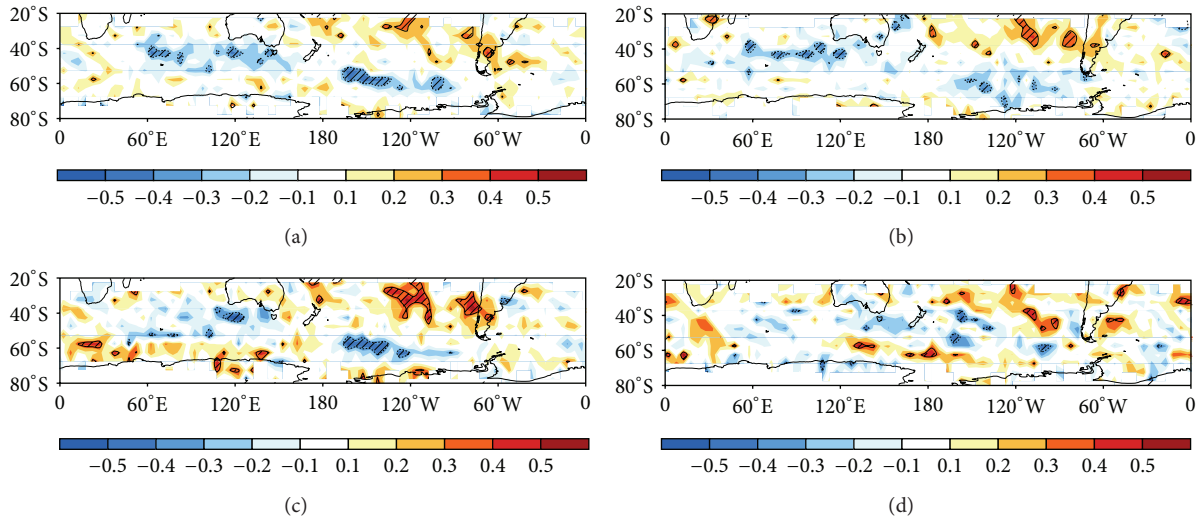

Figure 6: Partial correlation coefficient for cyclone frequency versus ENSO (excluding IOD) for SH Winter (JAS). Correlation (shaded), 2-Tail 90% significance (hatched) for (a) NCEP1_5801, (b) ERA40_5801, (c) NCEP1_7910, and (d) NCEP1_5078.

who used this method to isolate the impacts of IOD from ENSO on SH cyclone tracks. Since sea-level pressure is temporally discontinuous, we show results for frequency only and for NCEP1_5801 versus ERA40_5801 and NCEP1_7910 versus NCEP1_5078 to highlight differences between different reanalysis datasets and different temporal periods within the same reanalysis dataset, respectively. Consistent with Ashok et al. [11], El Niño correlations are conducted by filtering out the effects of the IOD; IOD correlations are conducted by filtering out the effects of El Niño, and AAO correlations are conducted by filtering out the effects of El Niño and the IOD. To highlight significance, regions with greater than 90% significance are computed via a 2-tailed test.

Figure 6 shows the partial correlation between El Niño and cyclone track frequency. The PSA pattern is apparent from the annular structure of correlations in the South Pacific, with positive (negative) correlations across the South Pacific centered between 30°S and 35°S (55°S and 60°S) across all reanalysis datasets (Figure 6). A portion of the equatorial Africa wave train may also be reflected by an area of negative correlation southwest of Australia (Figure 6). This area appears in all reanalysis datasets except for NCEP1_5078 (Figure 6(d)). When comparing NCEP1_5801 with ERA40_5801, the results look quite similar, although the band of negative correlation in the South Pacific is better defined for NCEP1_5801 (compare Figure 6(a) with Figure 6(b)).

The greatest differences are seen when comparing NCEP1_7910 with NCEP1_5078. In addition to the area of negative correlation southwest of Australia discussed above, differences between NCEP1_7910 and NCEP1_5078 include (1) a band of fairly weak negative correlation extending in a broken area from 55°S 170°W to 65°S 80°W in NCEP1_7910 but not in NCEP1_5078 and (2) a narrow zone of positive correlations evident in NCEP1_5078 from 65°S 120°W to 70°S 150°W but not in NCEP1_7910 (compare Figure 6(c) with Figure 6(d)). Although this may be related to the robustness of the ENSO/PSA teleconnection when comparing data prior to and after 1978, data assimilation is also a possible cause.

For the partial IOD correlation, a broken band of negative correlation at 40°S and a broken band of positive correlation at 60°S in the South Pacific eastward into the South Atlantic for NCEP1_5801 and ERA40_5801 correspond well to the equatorial Africa Rossby wave train discussed in the composite analysis (Figures 7(a) and 7(b)). Differences between NCEP1_5801 and ERA40_5801 include (1) a positive band of correlation at 60°S in the South Pacific defined best in NCEP1_5801 rather than in ERA40_5801, (2) an area of significant positive correlation at 60°S in the South Atlantic more prominent in NCEP1_5801 than in ERA40_5801, and (3) an area of positive correlation appearing in the South Indian Ocean between Africa and Australia in ERA40_5801 but not in NCEP1_5801 (compare Figure 7(a) with Figure 7(b)).

When comparing NCEP1_7910 with NCEP1_5078, differences in IOD response are noted by (1) bands of positive correlation south of Australia at 60°S and in the South Pacific between 30°S and 40°S in NCEP1_7910 but not in NCEP1_5078, (2) a broken band of negative correlation from east of Australia southeast to east of New Zealand which is displaced slightly equatorward in NCEP1_5078 relative to NCEP1_7910, and (3) significant positive correlations in the South Atlantic at 60°S in NCEP1_5078 but not in NCEP1_5801 (compare Figure 7(c) with Figure 7(d)). Although data assimilation is a possible contributor, the lack of a band of positive correlation along 60°S in the South Pacific in NCEP1_5078 suggests that the equatorial Africa Rossby wave train response to the IOD was better captured in the post-1978 period relative to the pre-1978 period.

Finally, the AAO correlation shows an annular structure, with a band of positive correlations centered at approximately 65°S and negative correlations at 50°S for all reanalysis datasets, especially over the South Indian Ocean (Figure 8). The AAO structure is better defined in NCEP1_5801 relative to ERA40_5801 consistent with our composite analysis

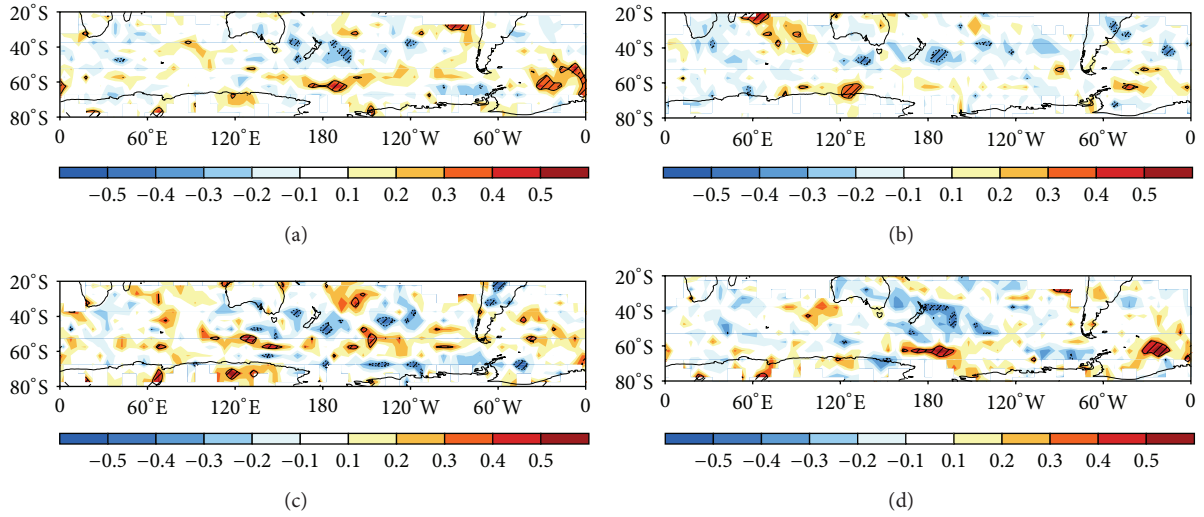

Figure 7: Partial correlation coefficient for cyclone frequency versus IOD (excluding ENSO) for SH Spring (OND). Correlation (shaded), 2-Tail 90% significance (hatched) for (a) NCEP1_5801, (b) ERA40_5801, (c) NCEP1_7910, and (d) NCEP1_5078.

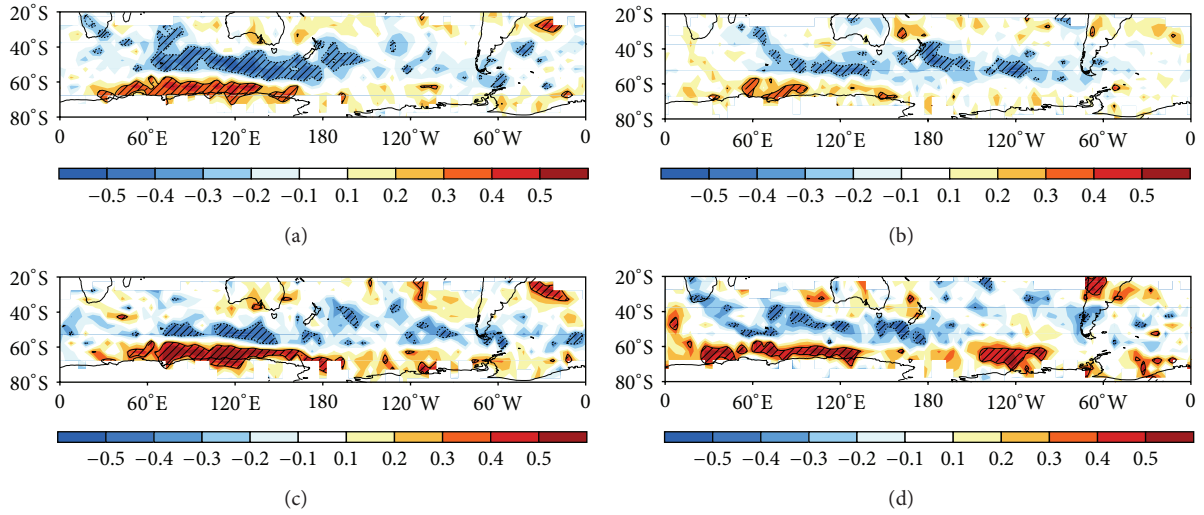

Figure 8: Partial correlation coefficient for cyclone frequency versus AAO (excluding IOD and ENSO) for SH Winter (JAS). Correlation (shaded), 2-Tail 90% significance (hatched) for (a) NCEP1_5801, (b) ERA40_5801, (c) NCEP1_7910, and (d) NCEP1_5078.

(compare Figures 8(a) and 8(b) with Figures 5(a) and 5(b)). The negative band in NCEP1_5801 along 50°S also extends westward to South Africa but not in ERA40_5801 (compare Figure 8(a) with Figure 8(b)). Although this difference may be due to model/assimilation differences between NCEP1_5801 and ERA40_5801, this feature is also seen in NCEP1_5078 (Figure 8(d)) suggesting that either data assimilation differences or differences due to a different AAO response may play a role.

Two interesting features are also noted when comparing NCEP1_7910 with NCEP1_5078 (Figures 8(c) and 8(d)). The first is an area of positive correlation east of Brazil in NCEP1_7910 but not in NCEP1_5078. The second is an area of positive correlation over northern Chile/northern Argentina/southwestern Brazil in NCEP1_5078. Regarding the first item, both differences in AAO response or differences in data assimilation are possible causes. Regarding point two, it is possible that, in addition to data assimilation differences, changes in lee-side cyclogenesis due to a positive trend in the AAO downwind of the Andes may also be responsible. Higher resolution reanalysis datasets will be beneficial in exploring this possibility.

6. Conclusions

All of the reanalysis datasets produced qualitatively similar frequency and intensity climatologies. Although there was no seasonal displacement in the location of cyclone tracks, there was a seasonal shift in magnitude for both frequency and intensity. When comparing cyclone track climatologies

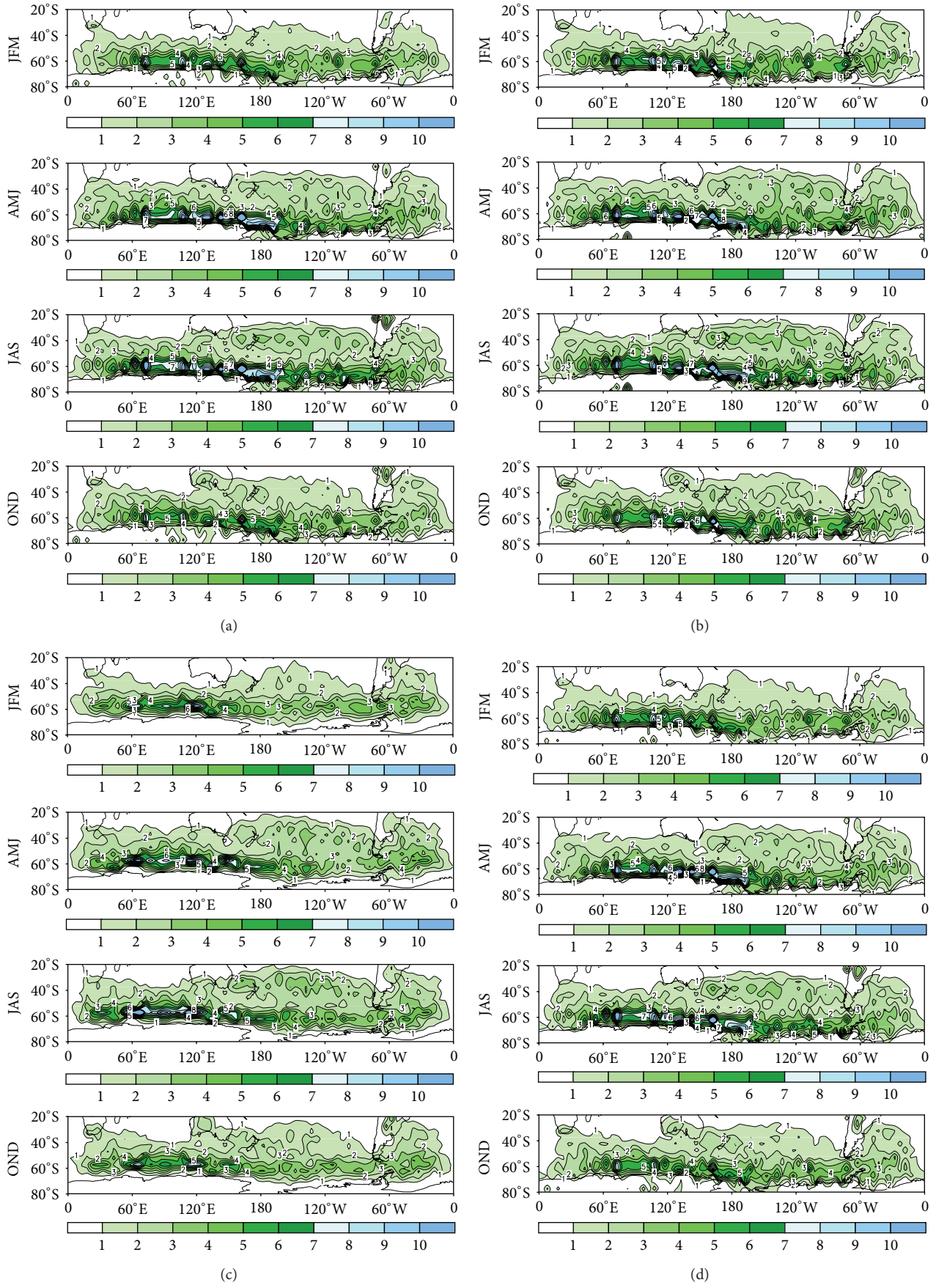

Figure 9: Continued.

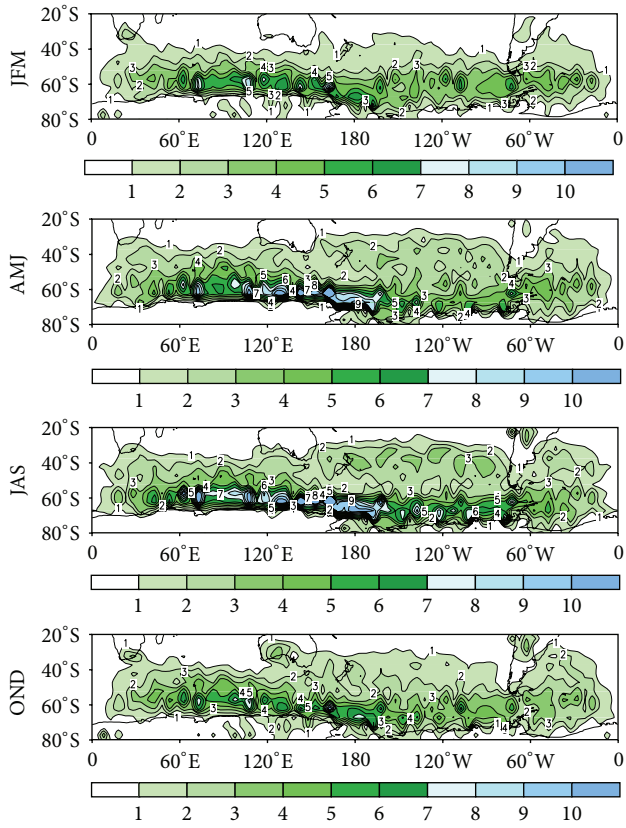

(e)

Figure 9: Southern Hemisphere seasonal cyclone track frequency climatology for (a) NCEP1_5801, (b) ERA40_5801, (c) NCEP2_7910, (d) NCEP1_7910, and (e) NCEP1_5078.

between datasets, NCEP2_7910 and NCEP1_7910 showed excellent agreement in their cyclone track frequency and intensity climatologies, which is not surprising given that this comparison was for an updated version of the same reanalysis dataset over the same temporal period. Systemic differences in frequency and intensity were attributed to either differences in data assimilation/model differences when comparing different reanalysis products for the same time period (e.g., NCEP1_5801 and ERA40_5801) or due to satellite data availability/climate changes (e.g., positive trend in the AAO since the 1970s) when comparing the same reanalysis product over different time periods (e.g., NCEP1_7910 and NCEP1_5078).

Composite analyses mapped well to several Rossby wave trains in several cases: namely, the PSA and equatorial Africa pattern for El Niño and the East Indian Ocean pattern for the IOD, demonstrating that surface based SH cyclone tracks respond to tropospheric changes due to anomalous convection in the tropics. Caution should be exercised, however, on using reanalysis data for regional climate assessments due to sensitivity from (1) coarse spatial gridding, (2) differences in assimilation techniques/models between reanalysis datasets, and (3) temporal period chosen for composite analysis. The AAO composites showed a robust annular structure for cyclone track frequency, but not in intensity, supporting the weak relationship between cyclone frequency and cyclone intensity discussed in Simmonds [57].

The Rossby wave structures seen in the composite analysis were also evident in the partial correlation analysis. This demonstrates that most likely several of the features evident in the composite analysis were not contaminated by other climate forcings. The absence of positive correlations along 60°S in the South Pacific in NCEP1_5078 suggests that the equatorial Africa Rossby wave train response to the IOD was less active prior to 1979.

Given the differences we see among the various reanalysis datasets in cyclone track climatology and interannual variability, it will be interesting to investigate how much improvement in consistency between datasets is gained when analyzing high resolution reanalysis datasets. Future work will focus on this task to see if our cyclone track methodology shows the same improvement for the SH as demonstrated by Hodges et al. [26]. Given the ability for the higher resolution datasets to reproduce storm structure, we also agree with Tilinia et al. [55] that it would be of great interest to examine the moisture content/transport related to midlatitude cyclones. Since assessing interannual variability in reanalysis datasets is always limited by sample size, it is not possible to do composite analysis for more than one climate variable. To address this, we also plan to utilize

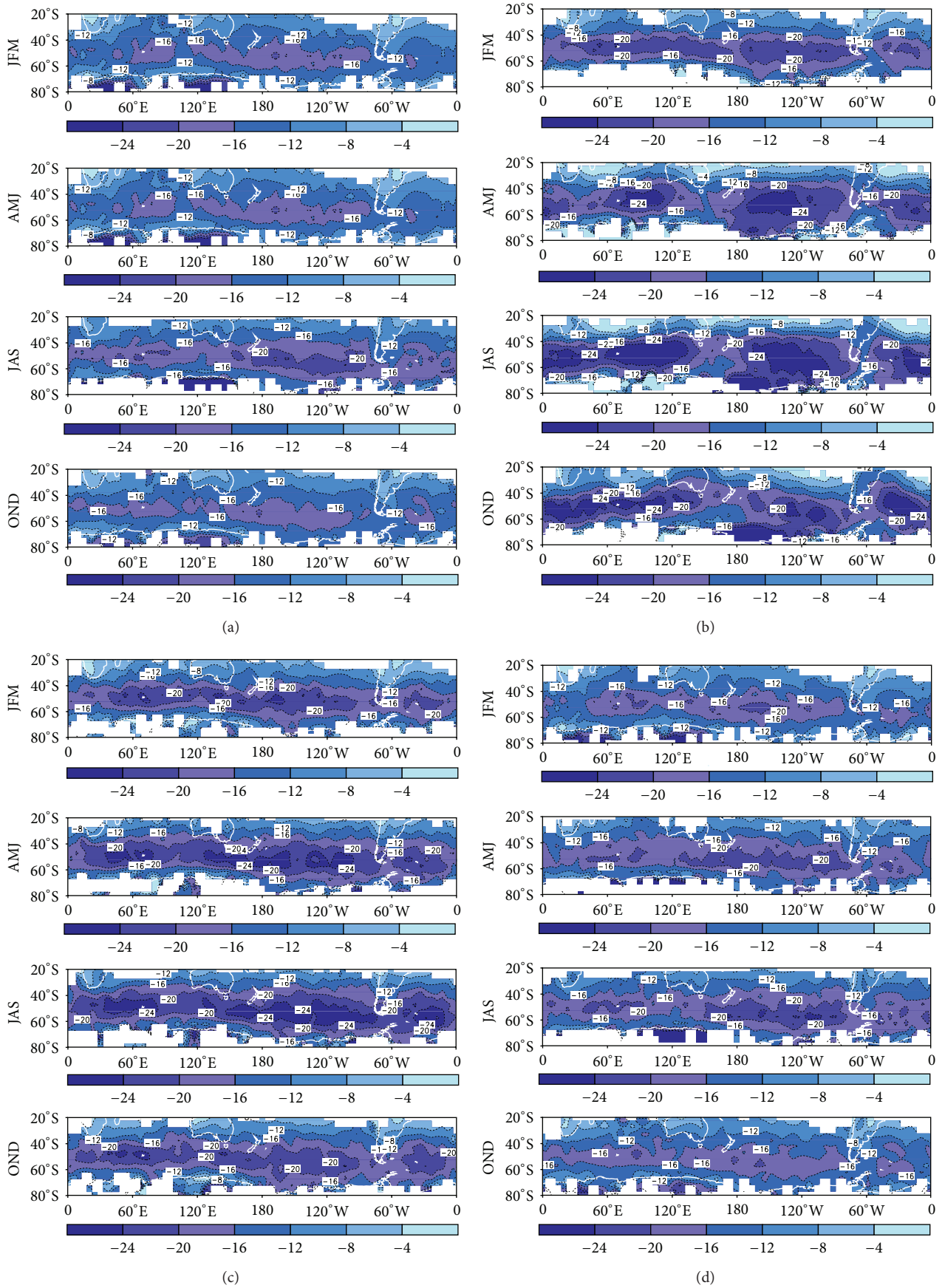

Figure 10: Continued.

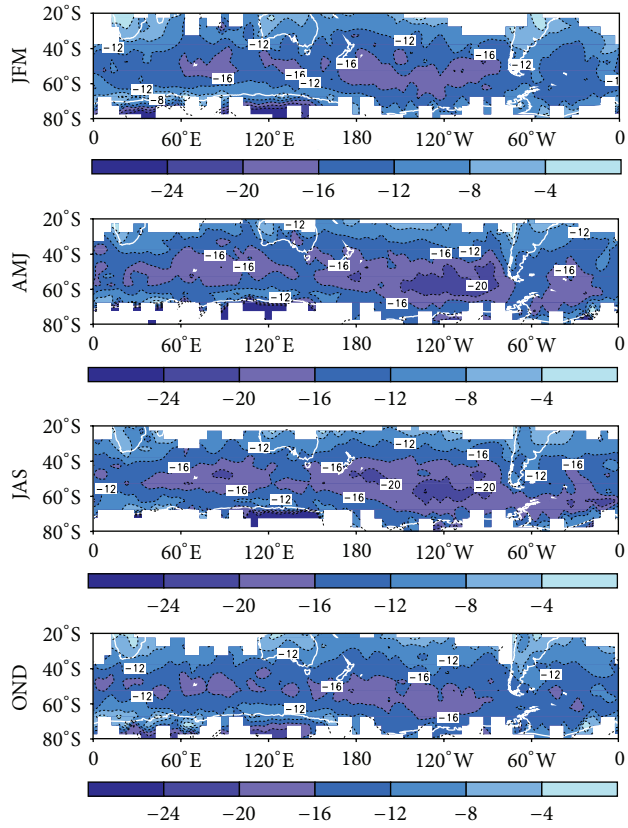

(e)

Figure 10: Southern Hemisphere seasonal cyclone track intensity climatology (JFM, AMJ, JAS, and OND) for (a) NCEP1_5801, (b) ERA40_5801, and (c) NCEP2_7910. Intensity calculated relative to seasonal mean sea-level pressure climatology. Units: hPa. (d) NCEP1_7910, (e) NCEP1_5078. Intensity calculated relative to seasonal mean sea-level pressure climatology. Units: hPa.

NCEP's reforecast data to construct statistically meaningful composites of combinations of El Niño-La Niña, IOD, AAO, and the PDO.

Conflict of Interests

Dr. Timothy Eichler and Mr. Jon Gottschalck declare that there is no conflict of interests regarding the publication of this paper.

References

[1] G. Midgley, R. Chapman, P. Mukheibir et al., "Impacts, vulnerability and adaptation in key South African Sectors," LTMS Input Report 5, Energy Research Centre, University of Cape Town, 2007.

[2] K. E. Trenberth, "Storm tracks in the Southern Hemisphere," *Journal of the Atmospheric Sciences*, vol. 48, no. 19, pp. 2159–2178, 1991.

[3] J. S. Frederiksen and C. S. Frederiksen, "Southern Hemisphere storm tracks, blocking, and low-frequency anomalies in a primitive equation model," *Journal of the Atmospheric Sciences*, vol. 50, no. 18, pp. 3148–3163, 1993.

[4] J. W. Kidson and M. R. Sinclair, "The influences of persistent anomalies on Southern Hemisphere storm tracks," *Journal of Climate*, vol. 8, no. 8, pp. 1938–1950, 1995.

[5] C. S. Frederiksen and J. S. Frederiksen, "A theoretical model of Australian northwest cloudband disturbances and Southern Hemisphere storm tracks: the role of SST anomalies," *Journal of the Atmospheric Sciences*, vol. 53, no. 10, pp. 1410–1432, 1996.

[6] E. H. Berbery and C. S. Vera, "Characteristics of the Southern Hemisphere winter storm track with filtered and unfiltered data," *Journal of the Atmospheric Sciences*, vol. 53, no. 3, pp. 468–481, 1996.

[7] V. B. Rao, A. M. C. do Carmo, and S. H. Franchito, "Seasonal variations in the Southern Hemisphere storm tracks and associated wave propagation," *Journal of the Atmospheric Sciences*, vol. 59, no. 6, pp. 1029–1040, 2002.

[8] M. Inatsu and B. J. Hoskins, "The zonal asymmetry of the Southern Hemisphere winter storm track," *Journal of Climate*, vol. 17, no. 24, pp. 4882–4892, 2004.

[9] H. Nakamura and A. Shimpo, "Seasonal variations in the Southern Hemisphere cyclone tracks and jet stream as revealed in a reanalysis dataset," *Journal of Climate*, vol. 17, no. 1, pp. 1828–1844, 2004.

[10] S. A. Solman and C. G. Menéndez, "ENSO-related variability of the Southern Hemisphere winter storm track over the Eastern

Pacific-Atlantic sector," *Journal of the Atmospheric Sciences*, vol. 59, no. 13, pp. 2128–2140, 2002.

[11] K. Ashok, H. Nakamura, and T. Yamagata, "Impacts of ENSO and Indian Ocean dipole events on the Southern Hemisphere storm-track activity during austral winter," *Journal of Climate*, vol. 20, no. 13, pp. 3147–3163, 2007.

[12] A. M. C. Carmo and E. B. de Souza, "The role of the sea surface temperature anomalies on the Storm Track behaviour during Southern Hemisphere summer," *Journal of Coastal Research*, no. 56, pp. 909–912, 2009, (Proceedings of the 10th International Coastal Symposium), Lisbon, Portugal.

[13] E. Lim and I. Simmonds, "Southern hemisphere winter extratropical cyclone characteristics and vertical organization observed with the ERA-40 data in 1979–2001," *Journal of Climate*, vol. 20, no. 11, pp. 2675–2690, 2007.

[14] A. B. Pezza, I. Simmonds, and J. A. Renwick, "Southern hemisphere cyclones and anticyclones: recent trends and links with decadal variability in the Pacific Ocean," *International Journal of Climatology*, vol. 27, no. 11, pp. 1403–1419, 2007.

[15] A. B. Pezza, T. Durrant, I. Simmonds, and I. Smith, "Southern hemisphere synoptic behavior in extreme phases of SAM, ENSO, sea ice extent, and Southern Australia rainfall," *Journal of Climate*, vol. 21, no. 21, pp. 5566–5584, 2008.

[16] D. Mendes, E. P. Souza, J. A. Marengo, and M. C. D. Mendes, "Climatology of extratropical cyclones over the South American-southern oceans sector," *Theoretical and Applied Climatology*, vol. 100, no. 3-4, pp. 239–250, 2010.

[17] X. Yuan, J. Patoux, and C. Li, "Satellite-based midlatitude cyclone statistics over the Southern Ocean: 2. Tracks and surface fluxes," *Journal of Geophysical Research D*, vol. 114, no. 4, Article ID D04106, 2009.

[18] B. J. Hoskins and K. I. Hodges, "A new perspective on Southern Hemisphere storm tracks," *Journal of Climate*, vol. 18, no. 20, pp. 4108–4129, 2005.

[19] U. Neu, M. G. Akperov, N. Bellenbaum et al., "IMILAST: a community effort to intercompare extratropical cyclone detection and tracking algorithms: assessing method-related uncertainties," *Bulletin of the American Meteorological Society*, vol. 94, pp. 529–547, 2013.

[20] M. G. Bosilovich, J. Kennedy, D. Dee, and A. O'Neill, *On the Reprocessing and Reanalysis of Observations for Climate, WCRP Position Paper, Version 1. 1*, WCRP, 2011.

[21] L. Bengtsson, S. Hagemann, and K. I. Hodges, "Can climate trends be calculated from reanalysis data?" *Journal of Geophysical Research D*, vol. 109, no. 11, Article ID D11111, 8 pages, 2004.

[22] E. Andersson, P. Bauer, A. Beljaars et al., "Assimilation and modeling of the atmospheric hydrological cycle in the ECMWF forecasting system," *Bulletin of the American Meteorological Society*, vol. 86, pp. 387–402, 2005.

[23] J. Chen, A. D. Del Genio, B. E. Carlson, and M. G. Bosilovich, "The spatiotemporal structure of twentieth-century climate variations in observations and reanalyses. Part I: long-term trend," *Journal of Climate*, vol. 21, no. 11, pp. 2611–2633, 2008.

[24] R. B. Rood and M. G. Bosilovich, "Reanalysis: data assimilation for scientific investigation of climate," in *Data Assimilation: Making Sense of Observations*, W. A. Lahoz, B. Khattatov, and R. Menard, Eds., Springer, 2010.

[25] K. I. Hodges, B. J. Hoskins, J. Boyle, and C. Thorncroft, "A comparison of recent reanalysis datasets using objective feature tracking: cyclone tracks and tropical easterly waves," *Monthly Weather Review*, vol. 131, pp. 2012–2037, 2003.

[26] K. I. Hodges, R. W. Lee, and L. Bengtsson, "A comparison of extratropical cyclones in recent reanalyses ERA-Interim, NASA MERRA, NCEP CFSR, and JRA-25," *Journal of Climate*, vol. 24, no. 18, pp. 4888–4906, 2011.

[27] H. Nakamura and T. Sampe, "Trapping of synoptic-scale disturbances into the North-Pacific subtropical jet core in midwinter," *Geophysical Research Letters*, vol. 29, no. 16, p. 1761, 2002.

[28] H. Nakamura, T. Izumi, and T. Sampe, "Interannual and decadal modulations recently observed in the Pacific storm track activity and èast Asian winter monsoon," *Journal of Climate*, vol. 15, no. 14, pp. 1855–1874, 2002.

[29] K. E. Trenberth, G. W. Branstator, D. Karoly, A. Kumar, N. Lau, and C. Ropelewski, "Progress during TOGA in understanding and modeling global teleconnections associated with tropical sea surface temperatures," *Journal of Geophysical Research C*, vol. 103, no. 7, pp. 14291–14324, 1998.

[30] B. Bhaskaran and A. B. Mullan, "El Niño-related variations in the southern Pacific atmospheric circulation: model versus observations," *Climate Dynamics*, vol. 20, no. 2-3, pp. 229–239, 2003.

[31] W. Cai, P. van Rensch, T. Cowan, and H. H. Hendon, "Teleconnection pathways of ENSO and the IOD and the mechanisms for impacts on Australian rainfall," *Journal of Climate*, vol. 24, no. 15, pp. 3910–3923, 2011.

[32] K. C. Mo and R. W. Higgins, "The Pacific South American modes and the tropical intraseasonal oscillation," *Monthly Weather Review*, vol. 126, pp. 1581–1596, 1998.

[33] R. D. Garreaud and D. S. Battisti, "Interannual (ENSO) and interdecadal (ENSO-like) variability in the Southern Hemisphere tropospheric circulation," *Journal of Climate*, vol. 12, no. 7, pp. 2113–2123, 1999.

[34] E. DeWeaver and S. Nigam, "On the forcing of ENSO teleconnections by anomalous heating and cooling," *Journal of Climate*, vol. 17, pp. 3225–3235, 2004.

[35] N. H. Saji, B. N. Goswami, P. N. Vinayachandran, and T. Yamagata, "A dipole mode in the tropical Indian ocean," *Nature*, vol. 401, no. 6751, pp. 360–363, 1999.

[36] N. H. Saji and T. Yamagata, "Possible impacts of Indian Ocean Dipole mode events on global climate," *Climate Research*, vol. 25, no. 2, pp. 151–169, 2003.

[37] K. Ashok, Z. Guan, and T. Yamagata, "Influence of the Indian Ocean Dipole on the Australian winter rainfall," *Geophysical Research Letters*, vol. 30, no. 15, p. 182, 2003.

[38] C. J. C. Reason and M. Rouault, "Links between the Antarctic Oscillation and winter rainfall over western South Africa," *Geophysical Research Letters*, vol. 32, no. 7, Article ID L07705, 2005.

[39] E. Kalnay, M. Kanamitsu, R. Kistler et al., "The NCEP/NCAR 40-year reanalysis project," *Bulletin of the American Meteorological Society*, vol. 77, no. 3, pp. 437–471, 1996.

[40] R. Kistler, E. Kalnay, W. Collins et al., "The NCEP-NCAR 50-year reanalysis: monthly means CD-ROM and documentation," *Bulletin of the American Meteorological Society*, vol. 82, no. 2, pp. 247–267, 2001.

[41] M. Kanamitsu, W. Ebisuzaki, J. Woollen et al., "NCEP-DOE AMIP-II reanalysis (R-2)," *Bulletin of the American Meteorological Society*, vol. 83, no. 11, pp. 1631–1643, 2002.

[42] S. M. Uppala, P. W. Kallberg, A. J. Simmons et al., "The ERA-40 re-analysis," *Quarterly Journal of the Royal Meteorological Society*, vol. 131, pp. 2961–3012, 2005.

[43] D. F. Parrish and J. C. Derber, "The National Meteorological Center's spectral statistical- interpolation analysis system," *Monthly Weather Review*, vol. 120, no. 8, pp. 1747–1763, 1992.

[44] P. Courtier, "The ECMWF implementation of three-dimensional variational assimilation (3D-Var). I: formulation," *Quarterly Journal of the Royal Meteorological Society*, vol. 124, no. 550, pp. 1783–1807, 1998.

[45] M. C. Serreze, "Climatological aspects of cyclone development and decay in the arctic," *Atmosphere*, vol. 33, no. 1, pp. 1–23, 1995.

[46] T. Eichler and W. Higgins, "Climatology and ENSO-related variability of North American extratropical cyclone activity," *Journal of Climate*, vol. 19, no. 10, pp. 2076–2093, 2006.

[47] D. W. J. Thompson and S. Solomon, "Interpretation of recent Southern Hemisphere climate change," *Science*, vol. 296, no. 5569, pp. 895–899, 2002.

[48] V. E. Kousky and R. W. Higgins, "An alert classification system for monitoring and assessing the ENSO cycle," *Weather and Forecasting*, vol. 22, no. 2, pp. 353–371, 2007.

[49] S. Nan and J. Li, "The relationship between summer precipitation in the Yangtze River valley and the previous Southern Hemisphere Annular Mode," *Geophysical Research Letters*, vol. 30, no. 24, p. 2266, 2003.

[50] D. Gong and S. Wang, "Definition of Antarctic oscillation index," *Geophysical Research Letters*, vol. 26, no. 4, pp. 459–462, 1999.

[51] I. Simmonds, K. Keay, and E. Lim, "Synoptic activity in the seas around Antarctica," *Monthly Weather Review*, vol. 131, no. 2, pp. 272–288, 2003.

[52] U. Ulbrich, G. C. Leckebusch, and J. G. Pinto, "Extra-tropical cyclones in the present and future climate: a review," *Theoretical and Applied Climatology*, vol. 96, no. 1-2, pp. 117–131, 2009.

[53] R. J. Murray and I. Simmonds, "A numerical scheme for tracking cyclone centres from digital data. Part II: application to January and July general circulation model simulations," *Australian Meteorological Magazine*, vol. 39, no. 3, pp. 167–180, 1991.

[54] M. G. Akperov and I. I. Mokhov, "A comparative analysis of the method of extratropical cyclone identification," *Izvestiya*, vol. 46, no. 5, pp. 574–590, 2010.

[55] N. Tilinia, S. K. Gulev, I. Rudeva, and P. Koltermann, "Comparing cyclone life cycle characteristics and their interannual variability in different reanalyses," *Journal of Climate*, vol. 26, pp. 6419–6438, 2013.

[56] J. Min, Q. Zhou, N. Liu, Q. Gao, and Z. Guan, "Teleconnection mode between IOD and Northern Hemisphere tropospheric circulation and its mechanism," *Meteorology and Atmospheric Physics*, vol. 100, pp. 207–215, 2008.

[57] I. Simmonds, "Modes of atmospheric variability over the Southern Ocean," *Journal of Geophysical Research*, vol. 108, p. 8078, 2003.